JOURNAL OF SPACECRAFT AND ROCKETS
Vol. 35, No. 5, September–October 1998

Analysis and Design of Aerocapture Tether with Accounting for Stochastic Errors

Steven G. Tragesser* and James M. Longuski†
Purdue University, West Lafayette, Indiana 47907-1282

As an alternative to conventional aerocapture spacecraft, a system comprising two vehicles (a probe and an orbiter) connected by a long thin tether has been proposed. In this tethered system, the probe provides the necessary atmospheric drag while the orbiter remains high above the sensible atmosphere. The results of a sensitivity analysis of the aerocapture tether are presented. Errors in knowledge of the atmosphere and in control of the initial conditions are considered. A result of the analysis is the discovery that the tethered system possesses a self-correcting mechanism that partially compensates for these errors. This intrinsic characteristic can be enhanced with a simple guidance algorithm that implements a change in the tether length to minimize the effect of off-nominal conditions. Design rules are developed to accommodate stochastic errors without violating the constraints, i.e., breaking or compressing the tether, subjecting the orbiter to atmospheric effects, crashing, or failing to capture. The final design consists of a 68-km tether with a mass of 381 kg and a probe and orbiter of 1000 kg each. It is capable of achieving a 99% success rate for aerocapture at Mars.

Nomenclature

A	= cross-sectional area, m^2
C_D	= drag coefficient
d	= tether diameter, mm
e_c	= eccentricity of target orbit about Mars
e_f	= eccentricity of final orbit about Mars
H	= atmosphere scale height, km
l	= tether length, km
l_{des}	= design tether length accounting for stochastic errors, km
l_{new}	= new tether length after reeling or unreeling, km
l_{nom}	= nominal tether length before reeling, km
m	= mass, kg
r_{per}	= target periapsis radius, km
r_{ref}	= reference density radius (from center of Mars), km
S_F	= safety factor for tether strength
$T_{\max}$	= maximum tether tension during aerocapture, N
$T_{\min}$	= minimum tension on the tether, N
V	= nominal velocity at periapsis, km/s
V_{inf}	= hyperbolic excess speed at Mars arrival, km/s
V_w	= wind velocity, m/s
α	= tether orientation angle, deg
α_c	= design constraint on tether orientation (less-dense case), deg
$\alpha_{\min}$	= minimum tether orientation angle during aerocapture, deg
$(\alpha_{\min})_{\text{des}}$	= tether orientation at periapsis for design, deg
$\dot{\alpha}$	= tether spin rate, rad/s
$\dot{\alpha}_{\text{new}}$	= new tether spin rate after reeling or unreeling, rad/s
$\dot{\alpha}_{\text{nom}}$	= nominal tether spin rate before reeling, rad/s
β_c	= design constraint of tether orientation (more-dense case), deg
ΔC_D	= perturbation of drag coefficient due to errors
Δh	= clearance (minimum altitude of orbiter minus minimum altitude of probe) during aerocapture, km
Δh_c	= minimum target clearance, km
$(\Delta r_{\text{per}})_{\text{eq}}$	= equivalent altitude change due to perturbation errors, km
Δr_{tot}	= required vertical displacement of probe to accommodate 99% of parameter uncertainties, km
$\Delta r_{\rho-}$	= required vertical displacement of probe to accommodate less-dense case, km
ΔV	= change in velocity, km/s
$\Delta\dot{\alpha}_0$	= perturbation to initial tether spin rate due to errors, rad/s
$\Delta\rho$	= perturbation to atmospheric density due to errors, kg/m^3
μ	= gravitational parameter, km^3/s^2
ρ	= atmospheric density, kg/m^3
ρ_{ref}	= reference atmospheric density at r_{ref}, kg/m^3
σ	= ultimate strength of tether, GN/m^2

Subscripts

f	= final state after aerocapture maneuver
o	= orbiter
p	= probe
t	= tether
0	= initial state before aerocapture maneuver

Received Nov. 10, 1997; revision received April 24, 1998; accepted for publication May 1, 1998.

*Ph.D. Candidate, School of Aeronautics and Astronautics; currently Technical Engineer, The Charles Stark Draper Laboratory, Inc., 555 Technology Square, Cambridge, MA 02139.

†Professor, School of Aeronautics and Astronautics. Associate Fellow AIAA.

Introduction

A GREAT deal of research has been focused on using aeroassist vehicles as a cost-effective means of deceleration, particularly at Mars. Unfortunately, significant uncertainty in the density of the Martian atmosphere can be expected because of a lack of data and short-period phenomena associated with solar activity and dust storms.[1,2] Also, navigation errors in the target periapsis altitude, although small on a celestial scale, lead to large changes in the atmospheric flythrough density. For a ballistic vehicle, these uncertainties may cause large deviations from the nominal orbit. One way to decrease the sensitivity to lack of knowledge and to delivery errors is to use propellant to achieve capture and then use aerobraking over multiple passes to circularize the orbit, as in the case of the Mars Global Surveyor,[3] which began its aerobraking in November 1997. Another option, which will be used by the Mars Surveyor '01 Orbiter, is to employ a feedback control scheme on a lifting body that can adjust the angle of attack for the variations encountered.[4–9] This paper explores a third option, the aerocapture tether concept.

Unlike a conventional ballistic vehicle, in the aerocapture tether concept, shown in Fig. 1, only a portion of the system (the probe) is subjected to aerodynamic drag; the other vehicle (the orbiter) is kept outside the atmosphere by the use of a long, thin tether.

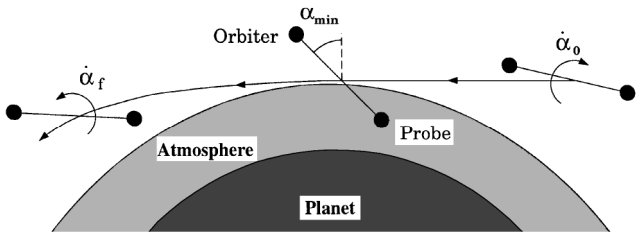

Fig. 1 Aerocapture maneuver.

The aerodynamic drag at the probe provides the ΔV necessary to capture the entire system, thereby eliminating the need for a large chemical burn at the orbiter. This aerodynamic drag produces a torque about the system center of mass that tends to plunge the orbiter into the atmosphere. To counteract this effect, the system approaches the planet spinning at a rate $\dot{\alpha}_0$ relative to the local vertical (Fig. 1). (Kowalsky and Powell[10] show that, by using pulsed ΔV during injection onto the interplanetary transfer, this rotational energy can be obtained with no additional propellant cost.) After the system enters the atmosphere, the spin rate decreases until it reaches zero near periapsis, at which point the system starts to spin up in the opposite direction ($\dot{\alpha}_f$). To minimize the tension on the tether, the magnitude of the spin rate leaving the atmosphere should be roughly equal to the spin rate entering the atmosphere.

There are numerous potential advantages of operating a tethered vehicle. First, the mass of the tether system may be less than that of a chemical rocket. Work by Puig-Suari et al.[11] demonstrates that, for deterministic cases, i.e., no stochastic errors, the tether mass is up to 76% less than the mass of the propellant needed for a present-day retrorocket. Furthermore, the tether is reusable, and so successive maneuvers can occur with no additional mass expenditure. (A mechanism for doing this without increasing the spin rate is discussed by Tragesser.[12]) The tether also can be used to collect dust from the Martian atmosphere,[13] to provide artificial gravity for manned missions, and to return samples or astronauts to Earth by serving as a sling.[14] These theoretical possibilities seem more likely now that deployment of long tethers has been achieved successfully by Tethered Satellite System (TSS)-1R and Small Expendable Deployer System (SEDS)-1 and SEDS-2, all to lengths of about 20 km (Ref. 15).

Under nominal conditions, the aerocapture tether has been demonstrated theoretically to adequately achieve aerocapture.[16–19] The next step in the feasibility analysis is to consider parameter uncertainties. We determine the effects of errors in the system parameters, e.g., atmospheric density, to ascertain whether the aerocapture tether is an operationally practical system. By carefully accounting for the stochastic errors, we are able to design a relatively simple aerocapture tether that should be able to achieve a high probability of mission success.

Obtaining the Nominal (Deterministic) Case

For our nominal (baseline) maneuver, we choose aerocapture at Mars with a final eccentricity of 0.90 to keep the mass of the tether low. (Tragesser et al.[20] show that the mass of the tether increases rapidly as e_f decreases.) We model the aerocapture tether using the formulation developed in Ref. 16. This model assumes that the tether is a rigid rod subjected to distributed aerodynamic and gravitational forces. (The work of Biswell et al.[17] shows that the flexible behavior of a carefully designed tether is benign and does not exhibit large perturbations from the rigid-rod model.) The three-degree-of-freedom (two translational, one rotational) model accounts for coupling between the attitude and the orbital dynamics of the system and assumes planar motion. (Reference 17 shows that out-of-plane effects are small.) The probe and orbiter are treated as particles. The atmospheric density profile is generated using Version 3.6 of the Mars Global Reference Atmospheric Model (Mars-GRAM).[21] We propagate the equations of motion using a Runge–Kutta–Verner fifth-order integrator.

We obtain the nominal maneuver using a numerical optimization technique developed in Ref. 22 that minimizes the tether mass. The formulation includes several constraints to ensure the success of the maneuver. First, the final eccentricity (after aerocapture) e_f must equal the eccentricity of the target orbit e_c. Next, the maximum tether tension during the maneuver T_{max} cannot exceed the ultimate strength of the tether (σA). Also, an inequality constraint is introduced so that the minimum altitude of the orbiter minus the minimum altitude of the probe (known as the clearance) Δh is greater than (or equal to) a set minimum, Δh_c. This ensures that the aerodynamic forces on the orbiter are insignificant. Finally, we require the minimum tension on the tether T_{min} to be nonnegative because compressive forces (negative tension) could cause severe bending in actual applications. The optimization problem is summarized by the following equations:

$$\begin{aligned} &\text{Minimize:} && m(\alpha_0, \dot{\alpha}_0, r_{per}, d, l) \\ &\text{subject to:} && e_f - e_c = 0 \\ & && T_{max} - \sigma A = 0 \\ & && \Delta h - \Delta h_c \geq 0 \\ & && T_{min} \geq 0 \end{aligned} \tag{1}$$

The solution to Eqs. (1) provides a tether mass of 87 kg for a specified clearance of 14.5 km and final eccentricity of 0.90. The nominal values for the parameters of the problem are given in Table 1. This list includes all of the initial conditions and system properties needed to simulate the maneuver except for the tether properties. The tether material is assumed to be Hercules AS4 graphite with a tensile strength of 3.6 GN/m^2 and a density of 1800 kg/m^3. Arrival conditions at Mars are determined by a Hohmann transfer from Earth. The spacecraft center of mass is set initially at a distance of 6170 km from the center of Mars, or approximately 20 min before periapsis encounter. For comparison, we note that the propellant mass required for an equivalent ΔV (to capture the orbiter) is 307 kg.

Table 1 Parameter values and uncertainties for aerocapture at Mars

Input	Nominal value	Variation,[a] 1σ	Ref.[b]
Orbiter mass	1,000 kg	±20 kg	7
Probe mass	1,000 kg	±20 kg	7
Tether mass	87 kg	±1 kg	7
Orbiter drag coefficient	2[c]	±0.1	7
Probe drag coefficient	1[d]	±0.1	7
Tether drag coefficient	2[c]	±0.1	7
Tether length	22 km	±0.2 km	——
Tether diameter	1.7 mm	±0.02 mm	——
Probe area	510 m^2	——	——
Orbiter area	10 m^2	——	——
Gravitational parameter	42,800 km^3/s^2	±400 km^3/s^2	——
Target periapsis altitude	91 km	±1.6 km	24
Wind velocity	0 m/s	±100 m/s	——
Density[e]	3.2×10^{-6} kg/m^3	±18%	21
Initial orientation angle	296 deg	±2 deg	——
Initial spin rate	−0.019 rad/s	$\pm 3.3 \times 10^{-5}$ rad/s	23
Hyperbolic excess speed	2.65 km/s	±1 m/s	9

[a]Normal distribution is assumed on all variables except density.
[b]Where no reference for the variation is given, engineering judgment is used to obtain a representative value.
[c]Free molecular flow is assumed.[13]
[d]Continuum flow is assumed.[13]
[e]From Mars-GRAM at a periapsis altitude of 84 km.

Parametric Uncertainties and Their Effects

The standard deviations for the parameters that govern the aerocapture maneuver are listed in Table 1. These uncertainties are based primarily on the literature for the current state of the art, but engineering judgment was required when data were unavailable. For example, in the case of the initial orientation angle, we recognize that a small deviation in the spin rate yields a large error in orientation over a duration of several hours or more. Thus, some autonomous control, e.g., changing the tether length, is required to reduce this error. We assume a control error of 2 deg as a conservative guess. The control error for the spin rate (0.33×10^{-4} rad/s) is based on the measurement accuracies easily obtainable with star sensors.[23]

We do not account for changes in the effective area of the probe and orbiter because they are assumed to be spherically shaped. For other geometries, the error in area can be absorbed by the drag coefficients because these two variables always appear together. The uncertainty in density is taken at an altitude of 84 km (from the Mars-GRAM model) because that is the altitude at which the probe flies through. Uncertainties in the drag on the tether at higher altitudes are less important because the total drag force on the tether is significantly lower than that of the probe. The control error in the target periapsis altitude can vary significantly depending on a number of factors, including the method of navigation, the length of the navigation arc, and the number of trajectory correction maneuvers. As a representative value, we use flight-path errors from the Mars Surveyor Mission[24] to obtain the 1σ value of 1.6 km. (Although this pushes the state of the art, we will see that the system is very sensitive to flight-path errors, and so this high level of accuracy is required.)

Our goal is to design a system that will have a 99% chance of success. We consider a mission successful if the following criteria are met: 1) the spacecraft is captured about Mars, 2) the tether does not break, 3) the orbiter maintains a minimum required altitude, 4) the spacecraft exits the atmosphere after the first flythrough, and 5) the tether does not compress. These requirements closely correspond to the constraints given in Eqs. (1). Assuming a normal distribution for the parameters of the problem, we must accommodate a range of $\pm 2.575\sigma$ to satisfy the mission constraints to a 99% probability. To evaluate the sensitivity of the aerocapture tether, the variables in Table 1 are perturbed from the nominal values by $\pm 2.575\sigma$ and a simulation is performed. The effect on the variables relating to the constraints in Eqs. (1) is shown in Table 2. Roughly half of the perturbations increase the ΔV of the flythrough, causing an increase in the tether tension and a decrease in the clearance. Because the nominal design barely satisfies tension and clearance constraints (with no margin), the tether breaks and the orbiter has unacceptable aerodynamic exposure in these cases. Other failure modes include low-density atmosphere and high-periapsis altitude, where the system is not captured ($e_f > 1$). Therefore, our nominal maneuver is not able to achieve a 99% success rate. To adequately redesign the system, we first focus on the dynamical behavior of the aerocapture tether.

Table 2 Simulation results for parameter uncertainties (2.575σ)

Variable	Perturbation	e_f	$T_{\max}$, N	Δh, km
Nominal case	0	0.900	7,890	14.5
Target altitude	+4.1 km	1.064	6,330	17.0
	−4.1 km	0.688	11,670	7.0
Density	+46%	0.745	10,720	8.7
	−46%	1.098	6,020	17.3
Probe drag coefficient	+0.26	0.818	9,630	11.0
	−0.26	0.994	6,890	16.7
Wind velocity	+260 m/s	0.857	8,720	12.8
	−260 m/s	0.942	7,470	16.1
Orbiter mass	+52 kg	0.910	8,190	14.4
	−52 kg	0.890	7,600	14.6
Tether length	+0.52 km	0.890	8,050	14.5
	−0.52 km	0.910	7,730	14.2
Probe mass	+52 kg	0.908	7,800	15.3
	−52 kg	0.893	8,160	13.7
Spin rate	$+8.5 \times 10^{-5}$ rad/s	0.893	8,440	13.2
	-8.5×10^{-5} rad/s	0.907	8,180	15.0
Tether drag	+0.26	0.897	7,920	14.5
	−0.26	0.903	7,930	14.5
Orientation	+5 deg	0.898	7,990	14.1
	−5 deg	0.902	7,990	14.9
Gravitational parameter	+1,000 km^3/s^2	0.901	8,470	14.4
	−1,000 km^3/s^2	0.901	8,660	12.5
Excess speed	+2.6 m/s	0.901	7,920	14.5
	−2.6 m/s	0.899	7,860	14.5
Tether mass	+2.5 kg	0.901	7,900	14.5
	−2.5 kg	0.899	7,900	14.5
Orbiter drag coefficient	+0.26	0.899	7,880	14.5
	−0.26	0.901	7,900	14.5
Tether diameter	+0.05 mm	0.899	7,900	14.5
	−0.05 mm	0.901	7,900	14.5

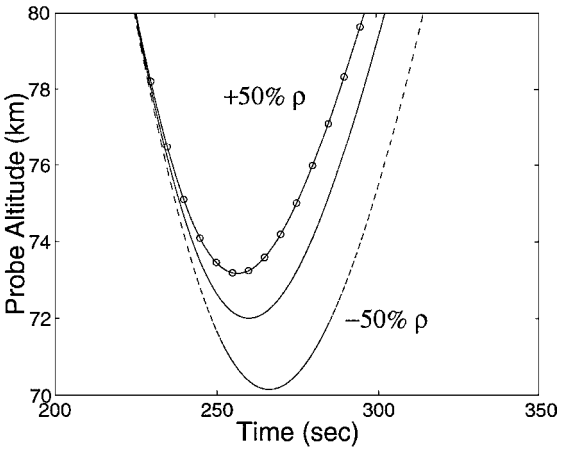

Fig. 2 Radial distance to the probe.

Robustness of the Aerocapture Tether

The tethered system provides some inherent compensation for parameter variations that is not present in an unguided aerocapture vehicle (modeled as a point mass). This inherent compensation is apparently due to the additional degree of freedom afforded by the rotation of the tether. Because the tether initially is spinning in the direction opposite to the orbital rotation, the ensuing dynamics serves as a self-correcting mechanism for any off-nominal conditions.

To illustrate, suppose the atmosphere is 50% less dense than expected or, equivalently, the target altitude is higher or the probe drag coefficient is smaller than the nominal. Then the resulting drag force, which is mostly on the probe, is insufficient to achieve the nominal ΔV. Fortunately, the lower density also reduces the torque, and so it takes more time for the spin rate to reach zero. As a result, the tether is more vertical near periapsis, i.e., $\alpha_{\min}$ is smaller, and the probe achieves a lower altitude than was targeted. This behavior is illustrated in Fig. 2, where the probe altitude for the −50% density perturbation reaches a minimum altitude that is about 2 km lower than the nominal. By flying through a lower altitude, the probe is exposed to a density that is closer to the nominal than the perturbed density at the nominal altitude. Conversely, if the atmosphere is denser than the nominal, the tether does not dip as deeply into the atmosphere, as shown in the trajectory for the +50% density of Fig. 2. This behavior partially offsets the effect of parameter uncertainties.

Guidance Scheme

It is possible to reduce the effect of parameter uncertainties even further if we actively target a specific orientation at periapsis rather than rely on the passive dynamics of the system. For instance, if the c.m. periapsis altitude is lower than expected, there exists a particular (more horizontal) orientation at closest approach that enables the probe to fly through the same-density altitude as the nominal trajectory (Fig. 3). If the tether length is sufficient, this result can be achieved while keeping the orbiter outside of the sensible atmosphere. Thus, employing a guidance scheme for the tether attitude allows the maneuver to obtain the nominal ΔV for off-nominal conditions.

To keep the system simple, the tether orientation at closest approach is controlled with a discrete change in the tether length during the approach trajectory. This control can be achieved by a reeling mechanism. By the law of conservation of angular momentum, the length change causes the new spin rate to be

$$\dot{\alpha}_{\text{new}} \approx \dot{\alpha}_{\text{nom}} (l_{\text{nom}} / l_{\text{new}})^2 \tag{2}$$

The modification in spin rate allows for a significant change in the flythrough orientation with a relatively small change in the tether length (implemented near the target planet but far away from the atmosphere). Resetting the initial conditions in this manner provides the foundation for the guidance algorithm.

This guidance scheme is simpler than using feedback control during the aerocapture maneuver, which may require an unreasonably fast reeling capability, but it requires knowledge of the perturbations

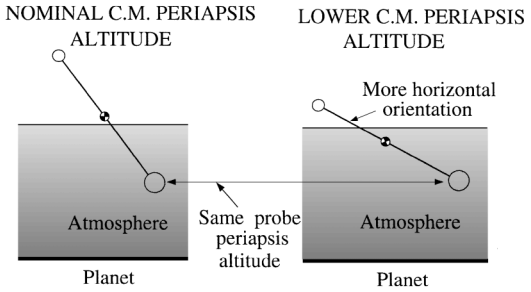

Fig. 3 Obtaining an equivalent probe flythrough altitude for off-nominal conditions.

before the maneuver occurs. Because perturbations in variables such as the probe ballistic coefficient and the density of the atmosphere are not known a priori, these uncertainties cannot be accommodated with this technique. However, errors in spin rate and target periapsis altitude can be measured to much higher precision than they can be controlled. As a result, by a suitable change in the tether length, we will be able to eliminate perturbations in ΔV caused by control errors in these variables.

Tether Design

Clearly the nominal tether system presented in Table 1 is incapable of accommodating the large uncertainties associated with aerocapture at Mars. Instead of designing the tether for nominal conditions, we need to incorporate the uncertainties into the design process. With this perspective, we first determine the extreme off-nominal conditions that the system may be subjected to for a given probability. For our goal of a 99% success rate, we use 2.575σ perturbations to construct the extreme case. The 2.575σ perturbations resulting in a larger ΔV than the nominal are given as the more-dense case in Table 3, and those resulting in a smaller ΔV are given as the less-dense case. To simplify the analysis, we first select only the variables that demonstrate significant importance in the sensitivity results of Table 2. In addition, the final design is sensitive to changes in spin rate, although the sensitivity to this variable is low for the case in Table 2, and so spin perturbations are included in the analysis.

To convert the separate uncertainties to a common metric, we assume that the periapsis drag force for the perturbed conditions is equal to the drag force for nominal conditions at some altitude $r_{\text{per}} + (\Delta r_{\text{per}})_{\text{eq}}$. Assuming an exponential atmosphere, we have

$$\frac{1}{2}(\rho_{\text{ref}} + \Delta\rho_{\text{ref}}) \exp\left(-\frac{r_{\text{per}} + \Delta r_{\text{per}} - r_{\text{ref}}}{H}\right) \times (V + \Delta V_w)^2 \left(C_{D_p} + \Delta C_{D_p}\right) A = \frac{1}{2}\rho_{\text{ref}} \exp\left[-\frac{r_{\text{per}} + (\Delta r_{\text{per}})_{\text{eq}} - r_{\text{ref}}}{H}\right] V^2 C_{D_p} A \tag{3}$$

The altitude change $(\Delta r_{\text{per}})_{\text{eq}}$ is an equivalent representation (to first-order approximation) of the perturbed conditions. Note that spin-rate perturbations are not included in this expression because they are eliminated using Eq. (2). Perturbations in spin rate are dealt with later. Solving for the equivalent altitude perturbation from Eq. (3) yields

$$(\Delta r_{\text{per}})_{\text{eq}} = \Delta r_{\text{per}} - H\left[\ln\left(1 + \frac{\Delta\rho_{\text{ref}}}{\rho_{\text{ref}}}\right) + \ln\left(1 + \frac{\Delta C_{D_p}}{C_{D_p}}\right) + 2\ln\left(1 + \frac{\Delta V_w}{V}\right)\right] \tag{4}$$

The equivalent altitude changes are shown in Table 3 for errors in density, probe drag coefficient, and wind velocity. The relative magnitudes of the equivalent altitude changes closely correspond to the relative size of the perturbations of eccentricity from Table 2. Thus, the ratio between these equivalent altitude changes can be used to estimate the change in e_f. To illustrate, we approximate the effect on e_f of a $+2.575\sigma$ error in ρ using the effect (from Table 2) of a -2.575σ error in r_{per}. Multiplying the e_f perturbation due to periapsis error, i.e., -0.212, by the ratio of the equivalent altitude perturbations from Table 3, i.e., 3/4.1, gives an estimated perturbation due to density error of -0.155 for an e_f of 0.745. This estimate matches the actual value found in Table 2 by simulating this error in density. The effects due to errors in the other variables are calculated using this same approach and are presented in Table 4. The estimated perturbations are very close to the values from the simulation, indicating that the equivalent altitude change is an accurate representation of perturbations to the other parameters.

Table 3 Perturbations for the extreme cases (2.575σ)

Case	Variable	Perturbation	Equivalent altitude perturbation	rss of perturbations
More dense	Δr_{per}	-4.1 km	-4.1	
	$\Delta\rho$	$+46\%$	-3.0	
	ΔC_{D_p}	$+0.26$	-1.8	-5.4
	ΔV_w	$+260$ m/s	-0.8	
	$\Delta\dot{\alpha}_0$	-8.5×10^{-5} rad/s	——	
Less dense	Δr_{per}	$+4.1$ km	$+4.1$	
	$\Delta\rho$	-46%	$+4.9$	
	ΔC_{D_p}	-0.26	$+2.4$	$+6.9$
	ΔV_w	-260 m/s	$+0.9$	
	$\Delta\dot{\alpha}_0$	$+8.5 \times 10^{-5}$ rad/s	——	

Table 4 Using equivalent altitude perturbations to estimate final eccentricity

		e_f	
Variable	Perturbation	Actual[a]	Estimated
Target altitude	$+4.1$ km	1.064	——
	-4.1 km	0.688	——
Density	$+46\%$	0.745	0.745
	-46%	1.098	1.096
Probe drag coefficient	$+0.26$	0.818	0.807
	-0.26	0.994	0.996
Wind velocity	$+260$ m/s	0.857	0.859
	-260 m/s	0.942	0.936

[a]From Table 2.

The variance for a sum of independent normal random variables is the sum of the variances, and so we obtain the total 2.575σ altitude perturbation by calculating an rss of the individual perturbations. This value, given in the last column of Table 3, represents the effective vertical distance that the system c.m. is displaced from the nominal height for the 2.575σ case. Therefore, to lessen the effect of a perturbation of this size, the probe must be capable of an altitude displacement that offsets the equivalent change in altitude of the c.m. The more-dense case, for example, requires that the minimum altitude of the probe must be raised 5.4 km (by an appropriate change in tether orientation) to achieve approximately the same ΔV as the nominal maneuver.

Accommodating 99% of the parameter perturbations clearly depends on having the capability of attaining vertical probe displacements from $+5.4$ to -6.9 km for a total of

$$\Delta r_{\text{tot}} = 12.3 \text{ km} \tag{5}$$

The tether must be long enough to encompass this range of vertical motion within a reasonable range of angular displacement. Obviously, the range of possible tether orientations at closest approach is limited to

$$0 \text{ deg} \leq \alpha_{\min} < 90 \text{ deg} \tag{6}$$

because compression occurs for negative values of the orientation angle and clearance cannot be obtained (even for very long tethers) if the system is horizontal at periapsis. In fact, the neighborhoods near these two extreme orientations have undesirable characteristics. Nearly vertical orientations result in large torques about the c.m., which cause large spin tensions and loss of clearance. Nearly horizontal maneuvers have large drag tensions and need very long

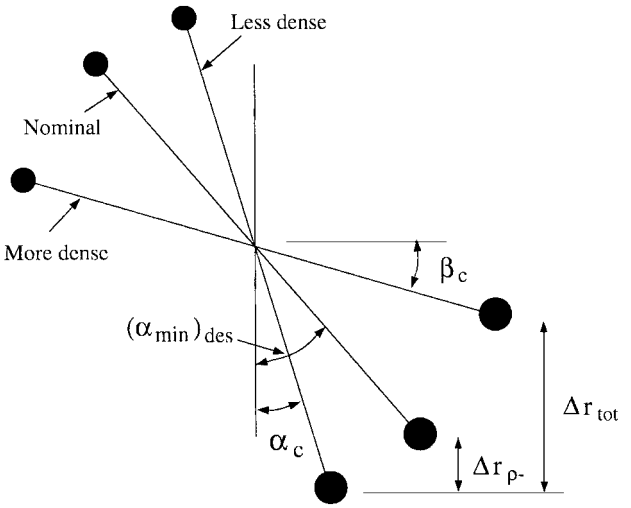

Fig. 4 Geometry of nominal and extreme cases.

tethers to achieve clearance. To avoid these cases, we enforce a more strict requirement, namely,

$$\alpha_c \leq \alpha_{\min} < \pi/2 - \beta_c \tag{7}$$

where α_c and β_c are shown in Fig. 4. Once these values are chosen, Δr_{tot} determines the design length l_{des} and periapsis orientation $(\alpha_{\min})_{\text{des}}$ of the tether. Using the law of sines, we find (from Fig. 4)

$$l_{\text{des}} = \frac{2\sin\left[\frac{1}{2}(\pi/2 + \alpha_c + \beta_c)\right]}{\cos(\alpha_c - \beta_c)\cos\left[\frac{1}{2}(\pi/2 + \alpha_c - \beta_c)\right]}\Delta r_{\text{tot}} \tag{8}$$

$$(\alpha_{\min})_{\text{des}} = \text{acos}[\cos(\alpha_c) - 2\Delta r_{\rho^-}/l_{\text{des}}] \tag{9}$$

where Δr_{ρ^-} is illustrated in Fig. 4.

With the tether length specified and the constraint on $\alpha_{\min}$ replacing the clearance constraint, the stochastic analog of the optimization problem described in Eqs. (1) is given by

$$\begin{aligned} &\text{Minimize:} && m(\alpha_0, \dot{\alpha}_0, r_{\text{per}}, d) \\ &\text{subject to:} && e_f - e_c = 0 \\ & && S_F T_{\max} - \sigma A = 0 \\ & && \alpha_{\min} - (\alpha_{\min})_{\text{des}} = 0 \\ & && T_{\min} \geq 0 \end{aligned} \tag{10}$$

Surprisingly, obtaining the nominal maneuver for stochastic errors is even simpler than it was in the deterministic case because of a reduction in the number of unconstrained states.

An estimate of the safety factor can be obtained by assuming that the tether will reach its maximum tension at periapsis. At this point, the spin rate is zero, and so the tension (assuming no tether drag) is equal to the axial component of the aerodynamic drag. Furthermore, application of the guidance scheme allows us to assume that the maximum drag is nearly constant for the perturbed cases. Then, the increase in maximum tension due to the more horizontal orientation of the more-dense case is found by simple geometry. Because the orientation at periapsis for the more-dense case is equal to $(\pi/2) - \beta_c$, the ratio between the maximum tension of the nominal and more-dense case is

$$S_F = \frac{\sin(\pi/2 - \beta_c)}{\sin[(\alpha_{\min})_{\text{des}}]} \tag{11}$$

Suitable values for α_c and β_c are obtained by iterating upon Eqs. (8–10) until a successful maneuver, by the criteria of Eqs. (1), can be found for the extreme cases in Table 3. Increasing α_c tends to make the maneuver more robust for the less-dense cases and increasing β_c helps decrease sensitivity to the more-dense cases.

Results

Our design of the aerocapture tether for the case of aerocapture at Mars has a final eccentricity of 0.90. Choosing

$$\alpha_c = 30 \text{ deg}, \qquad \beta_c = 29 \text{ deg} \tag{12}$$

we calculate the design length, minimum orientation, and safety factor from Eqs. (8), (9), and (11), respectively, to be

$$l_{\text{des}} = 65.7 \text{ km}, \qquad (\alpha_{\min})_{\text{des}} = 51.0 \text{ deg}, \qquad S_F = 1.13 \tag{13}$$

Using these values, we solve the parameter optimization problem expressed in Eqs. (10) to obtain the nominal maneuver for stochastic variables. The assumptions that the maximum tension occurs at periapsis and that the maximum drag is nearly constant are not accurate, and so we multiply the percentage increase in tether strength, i.e., 13%, by a factor of 3 (found iteratively) to yield a new safety factor of 1.40. This yields, by solving Eqs. (10), the final nominal design given in Table 5. The probe area of 200 m^2 has been determined by trial and error to minimize the normal forces in the tether, which minimizes bending when a flexible tether is considered.

This nominal maneuver is capable of satisfying Eqs. (1) for the extreme cases in Table 3 by implementing a length change of +2.1 and −3.2 km for the more- and less-dense cases, respectively, to target the appropriate orientation at periapsis. These tether lengths are found by solving for the root of the eccentricity constraint and then checking that the other constraints are satisfied. In the more-dense case, i.e., the greater ΔV case of Table 3, the tether is lengthened so that the spin rate decreases as dictated by Eq. (2). This results in a more horizontal orientation at periapsis, which raises the probe to the same density altitude as the nominal. Conversely, the length change for the less-dense case increases the spin rate so that the probe dips lower into the atmosphere.

Finding the length that satisfies Eqs. (1) for every maneuver is too computationally intensive if we want to assess the performance of the guidance scheme using a Monte Carlo simulation. To reduce the computational demands, we generated a grid of tether lengths for a range of perturbations and then interpolated for specific cases in the Monte Carlo simulation. Using a database in this fashion is a likely mode of operation for the guidance system. Contours of the tether length as a function of spin rate and periapsis altitude perturbations are shown in Fig. 5. To generate the plot, 297 data

Table 5 Final tether design

Parameter	Value
Tether mass[a]	368 kg
Clearance	40.9 km
Maximum force	8,010 N
Minimum tension	1,270 N
Probe area	200 m^2
Tether ultimate strength	11,220 N
Spin rate	−0.0069 rad/s

[a] An additional 2.3 km is required beyond the design length. This adds 12.9 kg to the total mass of the tether.

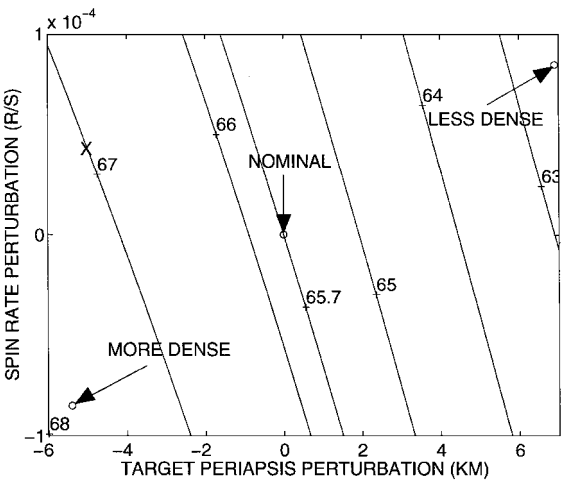

Fig. 5 Tether lengths for guidance algorithm.

points (27 × 11 grid) were used. The tether system is capable of achieving a successful maneuver for the entire range of perturbations shown, by lengthening or shortening the tether to the appropriate value. The more- and less-dense extreme cases from Table 3 are marked on the plot.

The range of tether lengths needed for the perturbations shown in Fig. 5 is from 62.8 km (upper-right-hand corner) to 68.0 km (lower-left-hand corner). Therefore, an additional 2.3 km is required beyond the design length, which adds 12.9 kg to the total mass of the tether.

We evaluated the performance of our final tether design by running 2000 cases in a Monte Carlo simulation. (See Ref. 25 for a similar analysis of the Pathfinder mission.) Perturbations were included for the inputs with the largest effects from the open-loop analysis: target periapsis altitude (or, equivalently, flight-path angle), atmospheric density, probe drag coefficient, wind velocity, and spin rate. Perturbations for all variables except density were generated by MATLAB for an assumed normal distribution with standard deviations from Table 1. To model atmospheric perturbations, we followed the approach used by Evans and Dukeman.[7] Using Mars-GRAM, which incorporates both random and wave perturbations for the density,[21] 100 density profiles were generated. (The density uncertainty is varied with altitude.) For the Monte Carlo simulation, a random number between 1 and 100 was generated, based on a uniform distribution, to determine which randomly generated Mars-GRAM profile would be used.

Only perturbations in the periapsis altitude and spin rate were assumed to be known because these can be measured much more accurately than they can be controlled. (Here we assume perfect knowledge of these two variables.) A discrete change in the tether length was made at the beginning of each trajectory based on these perturbations and on linear interpolation of the data in Fig. 5. By re-solving for the states (spin rate, periapsis orientation, and tether length) that meet the eccentricity constraint, we obtain the nominal ΔV for the estimated off-nominal conditions. For example, suppose an update on the state reveals that the r_{per} is 5 km lower than the nominal and the spin rate is in error by +0.000043 rad/s. Then, the tether would need to be unreeled to a length of 67.0 km as indicated by the × in Fig. 5. This changes the spin rate of the system according to Eq. (2). For this example the new spin rate of 0.0066 rad/s is slower than the nominal, and so the tether has a more vertical orientation at closest approach. A linear regression of the data in Fig. 5 provides the following guidance law:

$$l = -0.35\Delta r_{\text{per}} - 5400\Delta\dot{\alpha}_0 + 65.6 \tag{14}$$

which is accurate to within 0.4% and could be used as an alternative to linear interpolation of the guidance data.

Histograms of the Monte Carlo simulation are shown in Figs. 6–9, where the guidance scheme was implemented to offset stochastic errors. The final eccentricities for the 2000 cases are given in Fig. 6. The mean value of 0.903 is very close to the nominal, and aerocapture is obtained for a range of $\pm 2.9\sigma$. Only 10 of the 2000 cases are not captured at Mars. Although the eccentricities of many cases

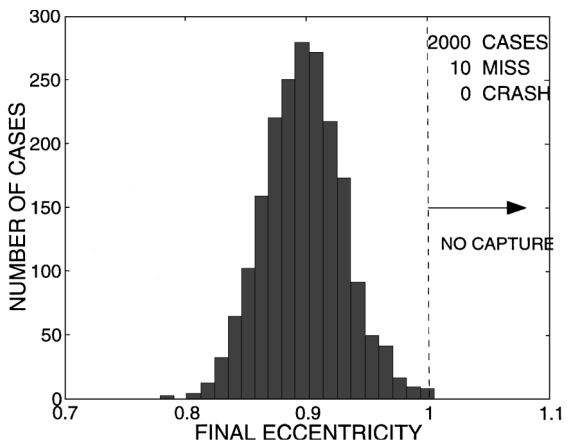

Fig. 6 Distribution of e_f for the aerocapture tether (μ = 0.903, σ = 0.033).

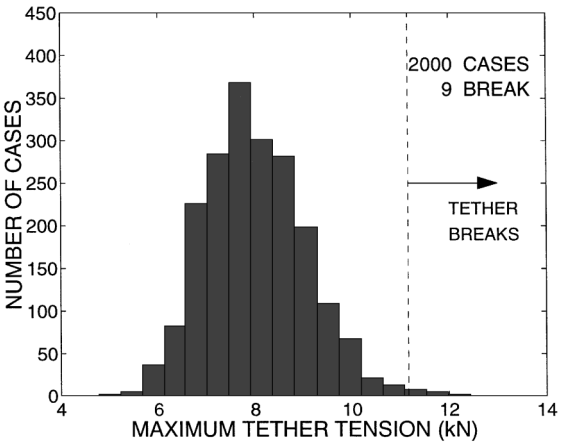

Fig. 7 Distribution of $T_{\max}$ for the tether (μ = 8210 N, σ = 1100 N).

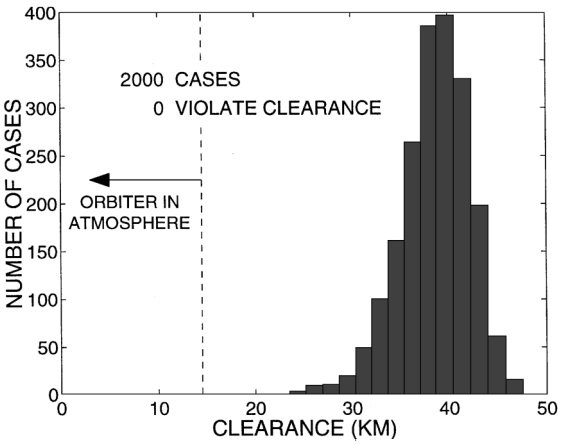

Fig. 8 Distribution of Δh for the tether (μ = 38.6 km, σ = 3.6 km).

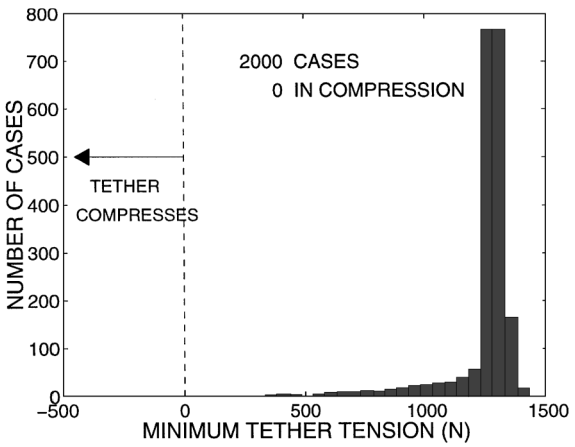

Fig. 9 Distribution of $T_{\min}$ for the tether (μ = 1220 N, σ = 140 N).

are near unity, 99% of the cases have a period less than 45 days and 96.1% have a period less than 10 days. A histogram of the maximum tension for each of the maneuvers is given in Fig. 7. Nine of the 2000 cases have a maximum tension that exceeds the strength of the tether. These cases probably could be eliminated by increasing the thickness of the tether, but the performance achieved here is sufficient for our goal. There are no violations of the clearance and compression constraints shown in Figs. 8 and 9. In fact, all of the cases achieve a clearance of three scale heights, which provides a large margin over the constraint value of 1.8 scale heights. In total, 19 of the 2000 cases violate one of the constraints, yielding a mission success probability of 99.1%.

A Monte Carlo simulation also was performed for the final tether design without implementation of the guidance algorithm, which corresponds to the failure (or absence) of the reeling mechanism so

that a change in the tether length is not possible. For the 2000 cases, the constant-tether-length performance yields 91 cases that do not achieve aerocapture, 16 cases in which the tether breaks, and 1 case that violates clearance. The overall mission success (for no reel) is 94.6%. (It seems clear that without the reel mechanism a mission success of 99% could be achieved at the cost of a more massive system, but we have not performed this analysis.)

The results in this paper demonstrate the feasibility and merit of the aerocapture tether, at least in theory. To more realistically assess the performance in an application, further refinements of the analysis would have to be considered. Here, we used a rigid-rod model for the tether and assumed perfect knowledge of the navigation errors, but flexibility effects and measurement errors may alter the results. For example, a large perturbation in density may cause some bending, which will increase the maximum tension in the tether. These effects should be small[17] and may be accommodated by increasing the tether safety factor.

Conclusions

We performed a sensitivity analysis of the aerocapture tether and found that the rotational degree of freedom afforded by the tether partially compensates for off-nominal conditions. To fully exploit this characteristic, we developed a guidance algorithm that reorients the flythrough attitude of the tether. Thus we can eliminate control errors using updated knowledge of the state. For example, a low-periapsis altitude can be offset by a more horizontal orientation of the tether. To evaluate the guidance scheme, we considered aerocapture at Mars, assuming available materials and state-of-the-art operational capabilities. The final design achieves a 99% probability of success, demonstrating the operational feasibility of the concept.

References

[1]Seiff, A., "Atmospheres of Earth, Mars, and Venus, as Defined by Entry Probe Experiments," *Journal of Spacecraft and Rockets*, Vol. 28, No. 3, 1991, pp. 265–275.

[2]Culp, R. D., and Stewart, A. I., "Time-Dependent Model of the Martian Atmosphere for Use in Orbit Lifetime and Sustenance Studies," *Journal of the Astronautical Sciences*, Vol. 32, No. 3, 1984, pp. 329–341.

[3]Lyons, D. T., "Aerobraking: The Key to Affordable Mars Exploration," Second International Academy of Astronautics International Conf. on Low-Cost Planetary Missions, IAA-L-0512, Laurel, MD, 1996.

[4]Gurley, J. G., "Guidance for an Aerocapture Maneuver," *Journal of Guidance, Control, and Dynamics*, Vol. 16, No. 3, 1993, pp. 505–510.

[5]Shipley, B. W., and Ward, D. T., "Robust Control Algorithms for Mars Aerobraking," *Advances in the Astronautical Sciences*, Vol. 79, Feb. 1992, pp. 633–652.

[6]Braun, R. D., and Powell, R. W., "Predictor-Corrector Algorithm for Use in High-Energy Aerobraking System Studies," *Journal of Guidance, Control, and Dynamics*, Vol. 15, No. 3, 1992, pp. 672–678.

[7]Evans, S. W., and Dukeman, G. A., "Examination of a Practical Aerobraking Guidance Algorithm," *Journal of Guidance, Control, and Dynamics*, Vol. 18, No. 3, 1995, pp. 471–477.

[8]Wercinski, P. F., and Lyne, J. E., "Mars Aerocapture: Extension and Refinement," *Journal of Spacecraft and Rockets*, Vol. 31, No. 4, 1994, pp. 703–705.

[9]McEneaney, W. M., and Mease, K. D., "Error Analysis for a Guided Mars Landing," *Journal of the Astronautical Sciences*, Vol. 39, No. 4, 1991, pp. 423–445.

[10]Kowalsky, C., and Powell, J. D., "Tethered Artificial Gravity Spacecraft Design," *Advances in the Astronautical Sciences*, Vol. 85, No. 1, 1993, pp. 645–664.

[11]Puig-Suari, J., Longuski, J. M., and Mechalas, J., "Aerobraking Tethers for the Exploration of the Solar System," *Acta Astronautica*, Vol. 35, No. 2/3, 1995, pp. 205–214.

[12]Tragesser, S. G., "Analysis and Design of Aerobraking Tethers," Ph.D. Thesis, School of Aeronautics and Astronautics, Purdue Univ., West Lafayette, IN, Dec. 1997.

[13]Pasca, M., and Lorenzini, E. C., "Optimization of a Low Altitude Tethered Probe for Martian Atmospheric Dust Collection," *Journal of the Astronautical Sciences*, Vol. 44, No. 2, 1996, pp. 191–205.

[14]Puig-Suari, J., Longuski, J. M., and Tragesser, S. G., "A Tether Sling for Lunar and Interplanetary Exploration," *Acta Astronautica*, Vol. 36, No. 6, 1995, pp. 291–296.

[15]Cosmo, M. L., and Lorenzini, E. C. (eds.), "Tether Flights," *Tethers in Space Handbook*, 3rd ed., Smithsonian Astrophysical Observatory, Cambridge, MA, 1997, pp. 1–20.

[16]Puig-Suari, J., and Longuski, J. M., "Modeling and Analysis of Orbiting Tethers in an Atmosphere," *Acta Astronautica*, Vol. 25, No. 11, 1991, pp. 679–686.

[17]Biswell, B. L., Puig-Suari, J., Longuski, J. M., and Tragesser, S. G., "Three-Dimensional Hinged-Rod Model for Elastic Aerobraking Tethers," *Journal of Guidance, Control, and Dynamics*, Vol. 21, No. 2, 1998, pp. 286–295.

[18]Puig-Suari, J., Longuski, J. M., and Tragesser, S. G., "Aerocapture with a Flexible Tether," *Journal of Guidance, Control, and Dynamics*, Vol. 18, No. 6, 1995, pp. 1305–1312.

[19]Longuski, J. M., Puig-Suari, J., Tsiotras, P., and Tragesser, S. G., "Optimal Mass for Aerobraking Tethers," *Acta Astronautica*, Vol. 35, No. 8, 1995, pp. 489–500.

[20]Tragesser, S. G., Longuski, J. M., and Puig-Suari, J., "A General Approach to Aerobraking Tether Design," American Astronautical Society/AIAA Astrodynamics Specialist Conf., AAS Paper 95-353, Halifax, NS, Canada, Aug. 1995.

[21]Justus, C. G., "A Mars Global Reference Atmospheric Model (Mars-GRAM) for Mission Planning and Analysis," AIAA Paper 90-0004, Jan. 1990.

[22]Tragesser, S. G., Longuski, J. M., and Puig-Suari, J., "Global Minimum Mass for Aerobraking Tethers," *Journal of Guidance, Control, and Dynamics*, Vol. 20, No. 6, 1997, pp. 1260–1262.

[23]Wertz, J. R., "Attitude Hardware," *Spacecraft Attitude Determination and Control*, 1st ed., Reidel, Dordrecht, The Netherlands, 1980, pp. 155–210.

[24]Kallemeyn, P., "Navigation Analysis Report for the Mars Surveyor '98 Lander," *Mars Surveyor '98 Project Mission Plan and Databook*, JPL Document M98-1-2001, Jet Propulsion Lab., California Inst. of Technology, Pasadena, CA, 1997, Appendix B.7.

[25]Spencer, D. A., and Braun, R. D., "Mars Pathfinder Atmospheric Entry: Trajectory Design and Dispersion Analysis," *Journal of Spacecraft and Rockets*, Vol. 33, No. 5, 1996, pp. 670–676.

F. H. Lutze Jr.
Associate Editor